Facet-specific Adsorption of Tri-peptides at Aqueous Au Interfaces: Open Questions in Reconciling Experiment and Simulation

Zak E. Hughes,* Raji Kochandra, and Tiffany R. Walsh*

Institute for Frontier Materials, Deakin University, Geelong, Vic. 3216, Australia

E-mail: zhughes@deakin.edu.au; tiffany.walsh@deakin.edu.au

Abstract

The adsorption of three homo-tri-peptides, HHH, YYY and SSS, at the aqueous Au interface is investigated, using molecular dynamics simulations. We find that consideration of surface facet effects, relevant to experimental conditions, opens up new questions regarding interpretations of current experimental findings. Our well-tempered metadynamics simulations predict the rank ordering of the tri-peptide binding affinities at aqueous Au(111) to be YYY > HHH > SSS. This ranking differs with that obtained from existing experimental data which used surface-immobilized Au nanoparticles as the target substrate. The influence of Au facet on these experimental findings is then considered, *via* our binding strength predictions of the relevant amino acids at aqueous Au(111) and Au(100)(1×1). The Au(111) interface supports an amino acid ranking of Tyr > HisA ≃ HisH > Ser, matching that of the tri-peptides on Au(111), while the ranking on Au(100) is HisA > Ser ≃ Tyr ≃ HisH, with only HisA showing non-negligible binding. The substantial reduction in Tyr amino acid affinity for Au(100) *vs.* Au(111) offers

one possible explanation for the experimentally-observed weaker adsorption of YYY on the nanoparticle-immobilized substrate compared with HHH. In a separate set of simulations, we predict the structures of the adsorbed tri-peptides at the two aqueous Au facets, revealing facet-dependent differences in the adsorbed conformations. Our findings suggest that Au facet effects, where relevant, may influence the adsorption structures and energetics of biomolecules, highlighting the possible influence of the structural model used to interpret experimental binding data.

Introduction

A comprehensive understanding of the structure/property relationships governing the biotic/abiotic interface, generated from a detailed knowledge of the interactions between biomolecules and materials interfaces, would deliver profound benefits in an enormous range of practical applications.[1–9] While the adsorption of peptides at the aqueous Au interface has been widely studied, our ability to predictably manipulate the structure of these biomolecules, and therefore their properties, when adsorbed at both planar surfaces and nanoparticle (NP) surfaces, under aqueous conditions, is still much needed. Despite several advances in this area in the past decade, the two key aspects regarding biomolecular adsorption at aqueous materials interfaces still require much deeper investigation and critical evaluation.

The first aspect is the reliable measurement of peptide-interface binding energetics, particularly the ability to quantitatively measure (or predict, in the case of molecular simulations) the binding free energy or binding constant. The second aspect is the ability to determine the conformational ensemble of the biomolecule in both the un-adsorbed and surface-adsorbed states. It is the latter that presents particular challenges for both experiment and simulation, but which is also integral to establishing structure/property relationships, and therefore facilitating the development of knowledge-based design of biomolecules for targeted

use in functional biotic/abiotic interfaces. Common to the successful interpretation of experimental and simulation data **covering both of these aspects** is the requirement of a physically-reasonable structural model of the substrate surface.

Determination of peptide-surface binding affinity for Au substrates under aqueous conditions has progressed from qualitative observations, *e.g.* fluorescence microscopy and ELISA (enzyme-linked immunosorbent assay) approaches, through to quantitative measurements such as surface plasmon resonance (SPR)[10–12] and quartz-crystal microbalance (QCM)[12–14] experiments. Electrochemical measurements[15] and other techniques[16] have also provided quantitative information about the amount of peptide adsorbed to the aqueous Au interface. Qualitative measurements that seek to link peptide-surface coverage (such as fluorescence microscopy), **or the amount of surface-adsorbed peptide mass,** with peptide-surface binding strength are particularly problematic and may lead to misinterpretations. This is due to the fact that peptide-surface coverage or adsorbed mass are associated not only with surface binding strength, but also the packing arrangements of the peptide over-layer when adsorbed on the surface. For example, a high coverage may arise for a given peptide sequence because the peptide adsorbs only *via* its terminus, which will typically correspond with a weaker surface-binding energy. Compare this with a peptide sequence that favors a horizontal planar adsorption orientation (which typically would have a stronger surface adsorption than the former) but would not necessarily support as dense a surface coverage.

In contrast, in the case of SPR or QCM observations, quantitative **binding constants** are the result of observations taken for several different peptide solution concentrations, **that are fitted to** *e.g.* a Langmuir model model. Moreover, use of dissipation measurements **with** QCM-D can establish the presence or absence of multi-layer peptide adsorption.[12,17] Key to the clear interpretation of these quantitative binding data, however, is a comprehensive compositional and structural characterization of the target substrate surface. Very few of the quantitative measurements mentioned **here** employed single-crystal Au surfaces; most used poly-crystalline Au or Au NPs, both of which present a range of crystallographic

orientations on the NP surface.

In contrast to the advances in determining **peptide-interface** binding energies, our ability to definitively characterize the conformational ensemble of the peptide in the surface-adsorbed state under aqueous conditions is much less developed. Specifically, experimental characterization of the molecular-level structure of adsorbed peptides/proteins under *in situ* (*i.e.* aqueous conditions) remains a challenging prospect. Atomic force microscopy (AFM) has been used to image the structure of peptide assemblies that have formed at dried Au interfaces.[18,19] However, AFM is unable to resolve the structure of the peptide chains at the desired level of detail. Moreover, it is likely that the drying process will affect the structure of the peptide assemblies. Likewise, electron microscopy approaches are similarly limited by the drawbacks of the latter. While advances in the use of *in situ* AFM under aqueous conditions are progressing for studying biomolecule adsorption,[20] this approach has yet to be reported for materials-binding peptides. A few recent studies have also reported use of techniques such as nuclear magnetic resonance (NMR) and sum frequency generation vibration spectroscopy to provide information about the structure of biomolecules adsorbed at aqueous interfaces.[21–24] While valuable, such studies are not yet part of standard analyses, and therefore obtaining unambiguous information on the structures of peptides adsorbed at aqueous interfaces remains challenging. The difficultly in obtaining structural information regarding adsorbed peptides is compounded by the fact that many materials-binding peptides are intrinsically disordered peptides (IDPs),[25,26] implying that these biomolecules cannot be adequately characterized by a single representative structure (or a few such structures) in the adsorbed state; on the contrary, these systems are better captured as an ensemble of structures. In summary, the ability to establish clear connections between the binding affinity of a peptide and the corresponding conformational ensemble characteristics of this peptide, in both the un-adsorbed and surface-adsorbed states, *via* experimental approaches alone, remains very limited to date.

Molecular simulation and computational chemistry can provide a crucial complementary

perspective on this problem.[4,12,13,27–45] Despite substantial progress in simulations of the peptide-Au interface, considerable challenges remain in terms of connecting the findings from molecular simulations to experimental data. To this end, three key conditions must be met for such molecular simulations to provide compelling insights; 1) a reliable **description of** the relevant inter-atomic interactions (particularly across the interface), 2) robust sampling of the conformational ensemble of the biomolecule, and, 3) an appropriate structural model of the target substrate surface. These three conditions are unavoidably inter-related and each one cannot be readily addressed in isolation. Progress in the area of inter-atomic potentials, referred to herein as force-fields (FFs), for describing biotic/abiotic interfaces has been substantial, notably (but not exclusively) the Au(111) interface, under aqueous conditions.[37,38,46,47] In particular, the development of the GolP FF provided a description of the interaction of the biomolecules/water with the Au(111) interface that incorporated polarization effects in addition to van der Waals interactions.[46] A revised version of GolP, the GolP-CHARMM FF,[37,38] was developed to enable compatibility with the CHARMM family of biomolecule FFs,[48,49] and was parametrized to capture adsorption at both the Au(111) and Au(100) interfaces (for the latter, in both native and reconstructed forms). Recently, GolP-CHARMM was used in the prediction of the binding free energy of a dodecapeptide at the aqueous poly-crystalline Au interface,[41] providing excellent agreement with SPR and QCM **binding constants**.

In parallel with advances in the development of new FFs, progress in enhanced conformational sampling approaches[43,50–52] have been integral to meeting the second main challenge listed above. Failure to adequately sample the conformational ensemble may give rise to misleading conclusions, as was demonstrated *via* a like-for-like comparison of the outcomes of regular MD simulation *versus* advanced sampling techniques for the adsorption of dodecapeptides.[12] The partnership of these new FFs and sampling techniques has considerably progressed our understanding of biotic/abiotic interface aqueous conditions.

However, for the interfacial FF and conformational sampling techniques to deliver useful

outcomes, the structural model used to approximate the biotic-abiotic interface must also be appropriate. In this sense, the structural model of the surface is a foundational component of any molecular simulation of the biotic-abiotic interface. Given the complexity of the conditions for which most experimental studies in this area have been reported, this structural model must, by necessity, be approximate. Provided the outcomes of the simulations are interpreted in light of this fact, the approximate nature of the surface structural model is not necessarily a severe limitation.

For example, to approximate the predicted binding affinity between a dodecapeptide (AuBP1) and the aqueous poly-crystalline Au interface, Wright et al.[41] calculated the free energy of peptide binding at both the Au(111) and Au(100) aqueous interfaces (in the latter case, for both the native and reconstructed forms), and used the known relative fractions of the two facets in poly-crystalline Au to construct a weighted average of these values. Critically, this **work** highlighted remarkable differences in peptide adsorption strength and adsorbed peptide structure depending on the reconstruction status of the Au(100) surface under aqueous conditions. In brief, these authors found that peptide adsorption at the Au(100)(5×1) interface was very similar to that of Au(111), while adsorption of the peptide at the aqueous Au(111) and native Au(100)(1×1) interfaces differed substantially. This difference was attributed to the greater degree of structuring of the interfacial solvent for the Au(100)(1×1) interface.[37,38,41,53] In terms of how these findings relate to experimental conditions, for planar poly-crystalline Au substrates under aqueous conditions, it is rather likely that the (100) **plane would** be present in **its** reconstructed form, for which the Au(100)(5×1) structure is an excellent model.[41] On the other hand, we note that the precise atomic structure of the {100} planes present on the surface of a faceted Au NP in aqueous solution (*i.e.* not under *in vacuo* conditions) remains to be resolved. Nevertheless, it is plausible that the {100} planes present on the surface of a faceted Au NP (of the dimensions used by Cohavi et al.[11]) may be stable in the Au(100)(1×1) form under aqueous conditions. Our view is informed by the in-plane row-slip deformation that is required to transform the

native Au(100)(1×1) surface into the reconstructed Au(100)(5×1) structure, which may be inhibited in Au NPs **due to** the small surface area of the facet in combination with the confining presence of the NP edges, at least for the NP sizes considered **by Cohavi et al**. Such considerations would not be as relevant for planar poly-crystalline Au substrates, where the surface area of Au(100) grains is anticipated to be substantially greater.

This distinction in the reconstruction status of Au(100) is critical, because previous work suggests that peptide adsorption to the aqueous Au(100)(5×1) interface is very similar to that on Au(111);[41] this suggests that a planar poly-crystalline Au substrate used in experiments (*e.g.* QCM measurements) can be reasonably approximated by molecular simulations using the aqueous Au(111) interface alone. In contrast, this same previous study indicated that peptide adsorption on Au(100)(1×1) is profoundly weaker than that on Au(111);[41] this finding indicates that consideration of native Au(100)(1×1) facets is essential when comparing molecular simulation data with adsorption experiments on faceted Au NPs, such as those reported in Cohavi et al.[11]. **To summarize, the evidence strongly suggests that adsorption onto small Au NP surfaces should not, in general, be viewed as adsorption onto a single-facet Au substrate.**

In addition, much of the complexity inherent to interpreting experiments and simulations of the peptide/Au interface arises from the fact that peptide adsorption cannot be viewed in simple terms as the sum of individual peptide residues that bind to the surface. The Au-interface binding affinity of a *residue* within a peptide will depend on the sequence and structure(s) of the peptide; this residue-based affinity may differ from the affinity of the individual *amino acid*. This may be due to local environment effects, *e.g.* the character of the residues that flank that particular binding residue.[12] Moreover, the lack of conformational control in these IDP-like systems contributes to these challenges. For this reason, while alanine scan experiments can be very valuable for elucidating peptide-materials binding,[54] the interpretation of these data can become obscure if the corresponding structural data of the adsorbed peptides are lacking.

Despite these complexities, a benchmark of amino acid binding affinities for aqueous Au interfaces, against which the binding propensity of a corresponding peptide residue could be evaluated, is of high value. While such benchmark data do not *per se* provide the detailed understanding or prediction of how strongly a given *peptide* sequence would adsorb to Au, these can help to bridge the gaps in our knowledge of how local peptide sequence effects can up- and down-modulate residue binding affinities,[54] compared to their amino acid counterparts. Ultimately, this level of understanding would advance the rational design of peptide sequences with material and/or facet selectivity.

Unfortunately, due to the reasons explained above, to date it has not been possible to extract an amino acid binding propensity scale for Au from experimental data regarding *peptide* adsorption, even for systems that consider homo-peptides (*vide infra*). In principle, this problem could be addressed by experimental observations of amino acid adsorption at aqueous Au interfaces, as opposed to measurement of peptide adsorption. In practice, the sensitivity of most QCM/SPR instruments is not sufficient for this purpose. Alternatively, the free energy of adsorption of Phe to the aqueous Au(111) interface was measured electrochemically, but with a considerable degree of uncertainty, between -18 and -37 kJ mol^{-1}.[15]

Experimental attempts to extract a Au-binding propensity scale for amino acids have instead used inference from measurements of the binding affinity of artificial sequences, such as homo-peptides, interdigitated sequences, and mutated sequences.[10,11,55–57] However, a number of these previous studies, particularly the more extensive surveys, used only qualitative binding assessments, *e.g.* fluorescence microscopy, which may not be sufficiently reliable for reasons explained earlier. Nevertheless, in a recent study that evaluated the current body of experimental work to date, Corni *et al.*,[36] reported an overall consensus derived from their evaluation that gave a non-covalent binding rank ordering of His $\approx$ Trp >Met > Tyr $\approx$ Lys $\approx$ Arg. Several molecular simulation studies have also attempted to generate amino acid binding propensity scales for aqueous Au interfaces. In these studies, the free-energies of

adsorption of amino acids to aqueous Au(111) can be calculated directly.[30,39,40] The consensus of these simulation studies indicates that the amino acids with the greatest non-covalent affinity to the aqueous Au(111) interface are Phe, His, Tyr, Trp, Met and Arg. Therefore, the general qualitative agreement between simulation and experiment for amino acid/Au binding is reasonable, and **indicates** that His, Trp, Tyr, Met and Arg have the greatest propensity to bind to Au.

However, a disconnect remains between experiment and simulation in terms of reconciling binding data for homo-peptides/mutants compared with those of the amino acids, for the reasons described above. Several previous studies have reported the calculation of the genuine free-energy of adsorption for peptide sequences (of length nine residues or greater) at a range of aqueous materials interfaces, predicted using advanced molecular simulations.[41,58–61] However, the computational cost of successfully completing such simulations for several peptides of **this size** becomes prohibitive, especially given the ambiguity over the atomic-scale structural model for the substrate surface, which even for a relatively simple system such as Au (compared with *e.g.* oxide materials), could involve the consideration of more than one surface **plane**. In light of this, short peptides, such as tri-peptides, adsorbed to well defined Au surfaces, comprise an ideal test case for both experimental and simulation approaches. The relative simplicity of these tri-peptides assures that their adsorption characteristics can be practicably explored using advanced sampling approaches.

Qualitative and quantitative experimental studies of tri-peptide **(and tri-peptide/protein fusion)** adsorption to aqueous Au surfaces have already been reported.[11] In this experimental study, Cohavi *et al.*[11] used SPR spectroscopy to quantify the binding affinity of a protein, TEM1-β-lactamase inhibitor protein (BLIP), at the aqueous Au interface. In addition to the wild-type protein (WT-BLIP), these authors also measured Au-surface binding for a protein construct where a homo-tri-peptide was fused to the N-terminus of the protein, denoted 3X-BLIP, where X covered the range of eighteen residues (**excluding** Cys and Pro). Their target Au substrate, however, was not a flat planar surface, but rather consisted of

faceted Au NPs immobilized onto the SPR chip surface. **Because** all of the proteins in their set showed irreversible adsorption (thus preventing the extrapolation of the binding constant, K_D), these authors devised a 'propensity scale' **based on the measurement of a quantity they termed 'binding potency'. However, we emphasize here that this 'binding potency' describes a difference in adsorbed mass, not binding strength (***vide supra***). We suggest that any such connection between binding constants and measurements of adsorbed mass alone should be interpreted with caution.** From **these differences in adsorbed mass, these authors** inferred that 3H-BLIP showed the greatest increase in '**binding potency**' relative to WT-BLIP.[11,43] In addition to 3H-BLIP, the 3X-BLIP proteins with enhanced '**binding potency**' relative to WT-BLIP also included X={W, K, M and Y}. Building on these findings, these authors used SPR spectroscopy **to measure the binding constant for a** set of free homo-tri-peptides (*i.e.* not fused to the BLIP protein) **namely** HHH, YYY and SSS, adsorbed at the Au NP-coated SPR surface. Their data suggested a ranking in **tri-peptide** binding strength of HHH > YYY > SSS,[11] however we note these binding constants were reported without any experimental uncertainties.

These authors investigated how their choice of Au **substrate** influenced the binding of the 3X-BLIP proteins, by comparing the binding *trends* obtained for the Au NP-decorated surface with **binding trends based on** textured Au(111) island surfaces, for X = {H, W, G and D} only. Cohavi *et al.* found that no qualitative differences in the '**binding potency**' trend for these four 3X-BLIP proteins was apparent for these two types Au **substrate**, and concluded that the Au NP-decorated surface must have primarily displayed the {111} facet. However, only the adsorption trends of the 3H-BLIP, 3W-BLIP, 3G-BLIP and 3D-BLIP systems were compared for the two types of target Au substrate. As our results herein indicate, the trends in Au-surface binding strength for a given set of residues may or may not be invariant to the Au facet displayed on the surface. Therefore, it is conceivable that the '**binding potency**' trends for the four 3X residue types considered in this cross-substrate

test (H, W, G, and D) were all actually broadly and moderately insensitive to facet type. In the absence of such a comparative test for the set of proteins {3H-BLIP, 3Y-BLIP, and 3S-BLIP}, **or preferably, actual binding constant measurements of the tri-peptides on different substrates**, it cannot be assumed that the conclusions reached by Cohavi *et al.* would hold for a comparison of the '**binding potency**' trend for the set of residues {H, Y and S}. **As will be explained in our Results,** the ambiguity of the protonation state of His, when part of a peptide residue (*vide infra*), particularly in the surface-adsorbed form, adds another degree of complexity to the interpretation of these findings.

To explore **the influence of facet type on the adsorption free energy (not adsorbed mass)**, here we investigated the structure and thermodynamics associated with the tri-peptides HHH, SSS, and YYY adsorbed at the aqueous Au interface, and compared these data against the experimental findings of Cohavi *et al.* First, the free energies of adsorption to the aqueous Au(111) interface were calculated for these three tri-peptides *via* well-tempered metadynamics simulations.[50] Following this, we again used metadynamics simulations to calculate the binding free energies of the Y, H **(both HisA and HisH)** and S amino acids, adsorbed at the aqueous Au(111) and Au(100)(1×1) interfaces. These amino acid data obtained for the different facets were contrasted with the adsorption free-energies of the tri-peptides, to provide guidance on the influence of Au facet type on the binding affinities. Finally, the conformational ensemble associated with each tri-peptide, adsorbed at both the Au(111) and Au(100)(1×1) interfaces, were predicted *via* the use of Replica exchange with Solute Tempering molecular dynamics (REST-MD) simulations.[51,52]

Methodology

The **Helmholtz** free energy of adsorption, ΔA_{ads}, was calculated for each of the three tri-peptides, HHH, SSS and YYY, adsorbed at the Au(111) surface under aqueous conditions using well-tempered metadynamics simulations.[50] The corresponding free energies of the

amino acids His, Tyr and Ser were also calculated for adsorption at the aqueous Au(111) and Au(100)(1×1) interfaces. For His, the adsorption free energy was calculated for both the positively-charged (HisH) and charge-neutral (HisA) forms of the amino acid. The conformational ensemble of each tri-peptide, adsorbed at both the aqueous Au(111) and Au(100)(1×1) interfaces, was determined using the REST-MD simulations. All MD simulations were performed in the Canonical (NVT) ensemble, with the temperature maintained at 300 K *via* use of the Nose-Hoover thermostat.[62,63] A time-step of 1 fs was used throughout, with the equations of motion integrated using the leap-frog algorithm.

System Setup

The interfacial interactions of the amino acids, tri-peptides and water with the Au(111) and Au(100)(1×1) surfaces were described using the polarizable GolP-CHARMM FF.[38] The CHARMM22* FF parameters[48,49] were used to describe the amino acids and tri-peptides, and the modified version of TIP3P,[64,65] compatible with the CHARMM FF, was used for the water molecules. For the tri-peptide simulations, the system consisted of an Au slab, presenting either the Au(111) or native Au(100)(1×1) surface, one chain of the tri-peptide, approximately 5100 water molecules, and in the case of the tri-His system (*vide infra*), a Cl^- counter ion. For the simulations of the capped amino acids, the system consisted of either an Au(111) or native Au(100)(1×1) surface, a single amino acid, $\sim$ 5000 water molecules, and for the positively-charged form of His, a Cl^- counter ion. All tri-peptides were modeled with their termini in the zwitterionic form, corresponding with pH$\sim$7. In the case of tri-His (HHH), the central H was protonated, such that this tri-peptide carried an overall charge of $+1e$. All four amino acids (Trp, HisA, HisH, and Ser) were capped with acetyl and N-methyl groups at the N- and C-termini, respectively. The Au(111) and Au(100)(1×1) surfaces were modeled using a slab five atoms thick, with lateral interfacial surface areas of $60.9 \times 58.6\,\text{Å}^2$ and $58.6 \times 58.6\,\text{Å}^2$, respectively. The positions of the Au atoms in the slab were fixed.[66] The dimension of the simulation cell along the direction normal to the slab surface was 60.5 Å

and 56.5 Å, for the Au(111) and Au(100)(1×1) surfaces, respectively. This ensured that the density of liquid water in the centre of the inter-slab space matched that of bulk liquid water calculated at the same ambient temperature and pressure.

REST Molecular Dynamics Simulations

The REST-MD simulations were performed using GROMACS version 5.0.[67] Full details of our REST simulation approach have been extensively described elsewhere.[4,51,52] Here, a set of sixteen replicas was used, spanning an effective temperature window approximately corresponding with the range 300-433 K. The Hamiltonian scaling values, λ, used for the sixteen replicas were 0.000, 0.057, 0.114, 0.177, 0.240, 0.310, 0.382, 0.458, 0.528, 0.597, 0.692, 0.750, 0.803, 0.855, 0.930, 1.000. These values were identified on the basis of previous simulations of peptides at aqueous Au interfaces.[12–14,39,41] **The initial conformations for the sixteen replicas of each tri-peptide were randomly selected from frames of the metadynamics simulations trajectories where the tri-peptide was adsorbed. The same sixteen conformations were used for both the Au(111) and Au(100)(1×1) simulations.** Each replica was equilibrated at its target Hamiltonian for 0.5 ns, with no exchange moves attempted during this period. For each of the three production REST-MD runs, the system was simulated for 15×10^6 REST-MD steps with exchanges attempted between neighboring replicas every 1000 time-steps (*i.e.* every 1 ps). The LJ-non-bonded interactions were smoothly tapered to zero between 10.0 and 11.0 Å, and the electrostatic interactions were evaluated using a particle-mesh Ewald summation,[68] with a real space cutoff of 11.0 Å. Figure S1 shows exemplar plots of replica mobility through Hamiltonian space, indicating the efficiency of sampling. **We used REST-MD simulations as an efficient way to gain a clear evaluation of the conformational ensemble of these surface-adsorbed tri-peptide systems, because our previous experience in using metaD-reweighting schemes for a surface-adsorbed dodecapeptide yielded ambiguous structural data depending on the re-weighting scheme used.[41] However, we recognize that such**

re-weighting schemes are evolving, as recently demonstrated by Sprenger et al.[69].

Metadynamics Simulations

We carried out two types of metadynamics simulations in this work. First, we performed metadynamics simulations of each tri-peptide adsorbed at the aqueous Au(111) interface. Second, we carried out metadynamics simulations of each of the four amino acids, adsorbed at both the aqueous Au(111) and Au(100)(1×1) interfaces.

The metadynamics simulations were performed using GROMACS version 4.5.5,[67] with version 1.3 of the PLUMED plugin.[70] The Lennard-Jones (LJ) non-bonded interactions were smoothly tapered to zero between 9.0 and 10.0 Å, and the electrostatic interactions were evaluated using a particle-mesh Ewald summation,[68] with a real space cutoff of 12.0 Å. The bias was applied to the position of the center of mass of the adsorbate (either the tri-peptide or the amino acid) along the direction perpendicular to the Au surface. Gaussians of 0.25 Å width were deposited every 1 ps. The initial height of the Gaussians was set to 1.5 and 0.5 kJ mol^{-1} for the tri-peptide and amino acid simulations respectively, and a well-tempered metadynamics bias factor of 10 was used throughout. The metadynamics simulations were run until the point that the resulting free energy profiles and adsorption free energies showed only minimal evolution with simulation time. This resulted in a production run for the amino acids of 250 ns, while for SSS, HHH and YYY the production simulations were of 500, 600, and 600 ns duration respectively. The adsorption free energies of Ser, Tyr and the charge-neutral form of His at the aqueous Au(111) interface, calculated using the GolP-CHARMM FF, were reported previously.[39] However, those previous metadynamics simulations used a different parameter (a Gaussian width of 1.0Å) and were run for a production duration of 100 ns. While the results of these previously-reported simulations are consistent with the current work, the free energy profiles obtained here study possess more fine detail due to the narrower Gaussians used. The free energies of adsorption as a function of simulation time are provided in Figure S2 of the Supporting Information, while Figure S3 provides

an exemplar evolution of the CV as a function of simulation time. In Figure S2 the free energy of adsorption at each point in time was calculated as the average of the ΔA values arising from adsorption at the upper and lower interface of the Au slab, while the error was determined from half the difference of the two values.

Analysis

Calculation of Adsorption Free Energies

Following Colombi Ciacchi and co-workers,[71] the Helmholtz free energy, ΔA_{ads}, of the tri-peptides and amino acids adsorbed at the Au surface was calculated from the free energy profiles generated by the metadynamics MD simulations using

$$\Delta A_{\mathrm{ads}} = -k_{\mathrm{B}}T \ln \frac{c_{\mathrm{ads}}}{c_{\mathrm{bulk}}} \tag{1}$$

where c_{ads} and c_{bulk} are the concentrations of the adsorbate in the surface-adsorbed and un-adsorbed (in bulk solution) states, respectively. These concentrations were calculated using

$$c_{z_0 \to z_1} = \frac{1}{z_1 - z_0} \int_{z_0}^{z_1} \exp(-A(z)/k_{\mathrm{B}}T) dz \tag{2}$$

We define z_0 and z_1 to demarcate the spatial limits of the regions in question. Here, the surface-adsorbed state was defined as those configurations where the adsorbate center of mass was no further than 20/15 Å from the slab surface for the tri-peptides/amino acids respectively. The bulk region was defined as the configurations that were found in the remaining inter-slab space. The final free energies of adsorption were then calculated by averaging over the last 200 ns or 75 ns of simulation time for the tri-peptides and amino acids, respectively. Uncertainties were estimated from the standard deviation over the same time periods.

REST Simulation Analyses

All analyses of the REST simulations were performed over the full length of the baseline trajectories (the trajectories of the replica corresponding to the un-scaled Hamiltonian). The degree of contact between a residue in the tri-peptide and the Au surface was determined by calculating the fraction of the baseline trajectory that the distance between a reference site in the residue and the Au surface was found within a pre-determined cut-off value. The residue reference sites were defined as the center of mass of the rings for His and Tyr, while the Ser site was defined as the hydroxyl oxygen atom. The cut-off distance for the Au(111) interface was set to 4.5, 4.3 and 4.0 Å for His, Ser, and Tyr, respectively. For the Au(100)(1×1) interface, two sets of cut-off distances were specified; one for direct contact and one for solvent-mediated contact. For His, Ser, and Tyr these values were set to 4.5, 4.5 and 4.2 Å, respectively for direct contact, and 6.0, 6.6 and 6.0 Å, respectively for solvent-mediated contact. These cut-off values were chosen on the basis of analysis of the histograms of distance of the residue contact site and the surface, as detailed in previous work.[12]

For each adsorbed tri-peptide, we characterized the Boltzmann-weighted ensemble of conformations according to similarity in backbone structure. We accomplished this using a clustering analysis determined for the peptide backbone atom positions, performed over the trajectory of the reference (un-scaled) replica trajectory. This analysis generates the set of most likely structures (referred to herein as 'clusters') and their corresponding relative populations in the ensemble. The Daura clustering algorithm was used here,[72] with a cutoff of 0.5 Å for the root mean-squared deviation (RMSD) of the backbone atom positions**, as determined from previous simulations.**[73] The relative population of each cluster was calculated as the percentage of the number of frames assigned to the cluster divided by the total number of frames in the reference replica trajectory.

Table 1: Comparison of adsorption free energies (kJ mol^{-1}) of three tri-peptides at the aqueous Au interface. Simulation data correspond with the aqueous Au(111) interface, while experimental results correspond with the Au NP-decorated SPR sensor surface.

Tri-peptide	Adsorption free energy	
	Simulation	Experiment[a]
HHH	-26.7 ± 2.5	-34.6
SSS	-2.9 ± 1.2	-20.2
YYY	-37.8 ± 2.2	-23.3

[a] Taken from Ref[11]

Results and Discussion

Adsorption Free Energies

The free energies of adsorption for the three tri-peptides (HHH, SSS, and YYY) at the aqueous Au(111) interface were obtained from well-tempered metadynamics simulations and are presented in Table 1, along with the relevant experimental data reported by Cohavi et al.[11]. The corresponding free energy profiles from the metadynamics simulations are shown in Figure 1. The free energies of adsorption as a function of simulation time are presented in Figure S2 of the Supporting Information; these data indicate that the free energies have stabilized after 500-600 ns of metadynamics simulation. As an exemplar, in Figure S3 in the Supporting Information we show the evolution of the CV as a function of simulation time; over the course of the metadynamics simulation the full range of the CV has been sampled extensively.

The data in Table 1 and Figure 1 indicate that HHH and YYY adsorb strongly to the aqueous Au(111) interface, while the the free-energy of adsorption of SSS is significantly weaker, of the order of $k_{\mathrm{B}}T$ at 300 K. The free-energy profiles for all three tri-peptides (Figure 1) are broad with no significant free-energy barriers to the adsorption from bulk solution. The ranking of the predicted free-energies of adsorption of the tri-peptides, YYY > HHH > SSS, was found to be the same as that predicted for the corresponding amino acids to aqueous Au(111) interface using both the GolP FF as previously reported by Hoefling

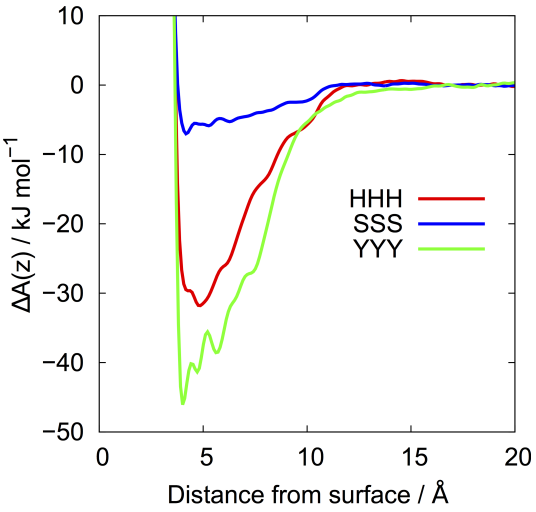

Figure 1: Profiles of the free-energy of adsorption for each tri-peptide, YYY, HHH and SSS at the aqueous Au(111) interface.

et al.[30], and the GolP-CHARMM FF (current work, *vide infra*).

However, the rank ordering of the tri-peptide binding free energies does not agree with that determined experimentally by Cohavi et al.[11], which was reported as HHH > YYY > SSS. Furthermore, the small difference (less than $k_{\mathrm{B}}T$ at room temperature) between the experimentally-determined adsorption free energies reported by Cohavi et al.[11] for YYY and SSS is unexpected, considering that the consensus of experimental data,[10,11,36,56] suggests that Tyr and His are strongly binding species, while Ser is not.

As explained in the Introduction, several factors may account for the differences, both absolute and relative, in the adsorption free energies obtained from experiment and those predicted from simulation; 1) the force-field used in the simulations, 2) the protonation state of His, and, 3) the structural model of the aqueous Au interface. First, the GolP-CHARMM FF used in our simulations is approximate and therefore may not reproduce the potential energy landscape of these interfacial systems adequately. However, **previously, this FF has yielded free energy predictions consistent with experimental data for the adsorption of Phe at aqueous Au(111),[12,39] and for the 12-mer peptide AuBP1 adsorbed at the aqueous poly-crystalline Au interface.[41]** Therefore, while it is not possible to completely exclude the quality of the GolP-CHARMM FF as a factor that could

account for differences between the simulation and experimental data, **current** evidence suggests that the GolP-CHARMM FF can provide a reasonable description of peptide-Au interactions.

The second possible factor is the protonation state of His. In the case of **tri-His**, the adsorption free energy predicted by simulation may be affected by the choice of protonation state of the His residues in the molecule. The experimental SPR measurements were reported to have been performed at pH 7.4.[11] Because the pK_a of the imidazole side-chain is $\sim$6.2 in the His *amino acid*, a His amino acid is expected to be found in both the protonated and un-protonated form at **around neutral** pH, with the protonated state making up $\sim$20% of the ensemble. It was for this reason that one of the His residues in **tri-His** was protonated in our simulations. However, the pK_a of a His *residue* within a peptide may differ from that of the corresponding His *amino acid*,[74] because the immediate dielectric environment of a residue in a peptide will depend on the conformational ensemble of the peptide. In addition, it is possible that the pK_a of a His residue in a peptide adsorbed at an aqueous Au interface may differ from the same His residue in a peptide when the peptide is in an un-adsorbed state (*i.e.* free in solution).

We emphasize here that this uncertainty concerning the protonation state of the imidazole ring becomes even more acute for tri-His in the Au-adsorbed state. To elaborate, it is more informative to consider tri-His not as one molecule in solution,[54] but as a mixture of eight possible distinct species; $(His_3)^{3+}$, $(His_3)^{2+}$ (three structural variations), $(His_3)^{1+}$ (three structural variations), and $(His_3)^0$. At equilibrium, the relative proportions of these eight species are expected to be a function of pH, but the precise relative fractions of these in the overall ensemble, particularly in the Au-adsorbed state, are not known. For example, the protonation state of tri-His was not determined or reported in Cohavi et al.[11] Moreover, assuming that the shifts in the pKa of the imidazole ring are not excessively profound at around neutral pH for tri-His in the surface-adsorbed

state, the overall composition of this ensemble of protonation states (*i.e.* in terms of the relative fraction of each protonation state) may well show large variations with respect to very small changes in pH in this neutral range. Experimental advances are much needed to unambiguously determine the relative fraction at equilibrium of these protonation states in tri-His and similar poly-His peptides. Therefore, the difference in the relative order of the adsorption free energy of **tri-His** and **tri-Tyr** between simulation and experiment might be due to the protonation state of tri-His modeled here.

The third factor that could explain the differences between the experimental and predicted adsorption free energies is the structural model of the Au interface, particularly the possible structural differences between the Au substrate used in the simulations and that used in the corresponding experiments. The SPR measurements used to obtain the experimental adsorption free energies used a SPR chip decorated with Au NPs as the substrate.[11] The exterior of these Au NPs, 4-7 nm in diameter, would have presented a range of different facets, as well as low-coordinate Au atoms at edge and vertex sites. In contrast, our metadynamics simulations of the tri-peptides were performed using the planar Au(111) aqueous interface. Previous simulation studies have indicated that the adsorption of molecules at different facets can differ.[29,31,37,38,41] For example, the aforementioned study of Wright et al.[41] predicted the adsorption free energies of AuBP1 to the Au(111) and native Au(100)(1×1) interfaces as -51.8 ± 18.1 and -10.3 ± 1.5 kJ mol^{-1}, respectively. One of the main factors attributed to these very different adsorption energies was the interfacial solvent layer closest to the surface, which was noted to be more tightly structured for the Au(100)(1×1) interface, compared with that of Au(111).[38,41] This observation has been noted for the aqueous interface of other fcc metals.[53,75] Therefore, it is plausible that the presence of other facets on the Au NPs (immobilized on the SPR chip surface in the experiments of Cohavi et al.[11]) may be responsible**, in part,** for the differences noted for the tri-peptide adsorption free energies determined by experiment and simulation. We re-iterate here that, in contrast, Wright

Table 2: Adsorption free energies, ΔA_{ads}, of capped amino acids to the aqueous Au(111) and Au(100)(1×1) interfaces.

amino acid	ΔA_{ads} / kJ mol^{-1}	
	Au(111)	Au(100)
HisA	-12.8 ± 0.9	-6.0 ± 1.8
HisH	-10.9 ± 0.7	-0.3 ± 2.5
Ser	-3.6 ± 1.1	-1.4 ± 0.1
Tyr	-19.5 ± 1.5	-0.8 ± 0.4

et al.[41] also reported that the reconstructed Au(100)(5×1) surface, likely to be present on the surface of poly-crystalline Au under aqueous conditions, supported peptide binding energies and conformations that were very similar to those found for aqueous Au(111).

To investigate both the impact of His protonation state, and the influence of the different Au facets on the binding free energy of His, Ser and Tyr, the adsorption free energies of the capped amino acids were calculated for both the aqueous Au(111) and Au(100)(1×1) interfaces. We used the capped amino acids as our choice of adsorbate, rather than the tri-peptides, because this substantially reduced the computational cost of these simulations. **This is particularly true for the tri-His case, which conceivably would involve performing a weighted average over the results of eight different metadynamics simulations, and moreover, the fractional weighting of these eight possible protonation states for the relevant solution pH is currently not known**. This allowed both comparison between the tri-peptide and the corresponding amino acid adsorption at the Au(111) interface, and also enabled the influence of histidine protonation to be more clearly **explored**. The amino acid adsorption free energies are given in Table 2. The rank ordering of these adsorption free energies at the aqueous Au(111) interface is the same as **that predicted** for the tri-peptides, Tyr > HisA $\simeq$ HisH > Ser, with the **de**-protonated form of His (HisA) having a slightly stronger binding than the protonated form (HisH). In contrast, at the aqueous Au(100)(1×1) interface, the free-energies of adsorption of HisH, Ser and Tyr are all negligible, with only HisA showing a significant adsorption free energy, albeit modestly reduced compared to the Au(111) interface.

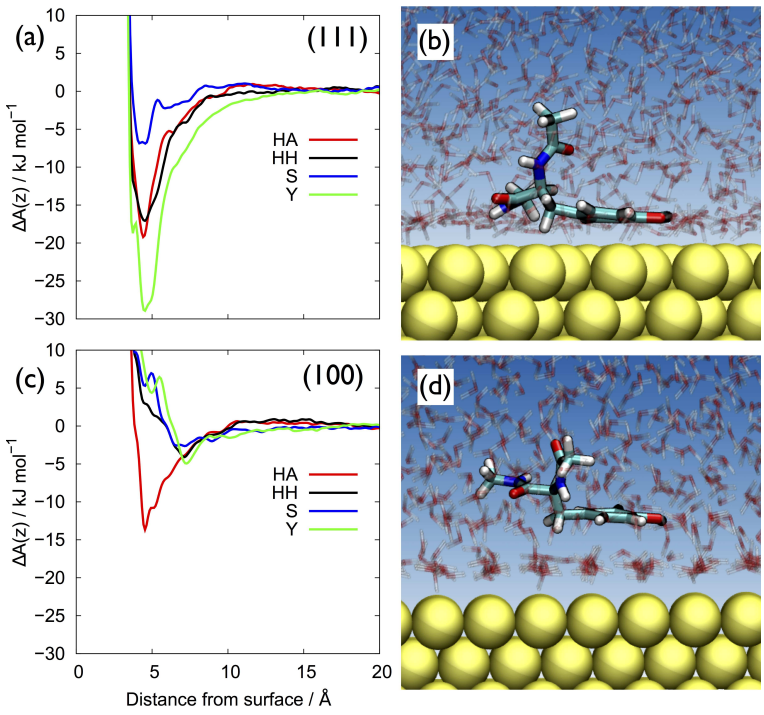

Figure 2: Profiles of the free energy of adsorption of the capped amino acids at (a) the Au(111) interface, and (c) the Au(100)(1×1) interface. Corresponding representative snapshots of the adsorbed state of Tyr at (b) the Au(111) interface, and, (d) the Au(100)(1×1) interface.

Following previously-published studies,[37,41,53,75] we suggest that the difference in binding energies between the two interfaces is due to the greater degree of structuring in interfacial liquid water that is present at the Au(100)(1×1) interface, compared with the Au(111) interface. At the aqueous Au(111) interface the minimum in the free energy profile for the amino acids, see Figure 2(a), is ∼4.5 Å from the surface. This corresponds to a conformation where all four amino acids are in direct contact with the Au interface, as shown in Figure 2(b) and Figure S4 in the Supporting Information. Our findings are very different for the aqueous Au(100)(1×1) interface, where only in the case of HisA does the free energy minimum correspond to direct contact between the amino acid and the surface. For the other three amino acids, the minimum in the free energy profiles corresponds to 'solvent-mediated' adsorption (Figure 2(c)). In this solvent-mediated contact state, the amino acid is adsorbed onto the first layer of interfacial water (Figure 2(d) and Figure S4). This scenario

would make it less enthalpically favorable for the adsorbate to displace water molecules. The charge-neutral HisA amino acid is an exception, due to the very favorable interaction between the **de**-protonated nitrogen site in the imidazole ring and the Au surface atoms.

This difference in adsorption modes at the two Au interfaces confers differences in the structure(s) of the surface-adsorbed His, depending on the protonation state of the His and crystallographic orientation of the Au surface. The positively-charged HisH amino acid adsorbed in a manner analogous to Tyr, predominantly with the plane of the side-chain ring oriented parallel to the Au surface. However, in the case of HisA, two possible adsorption geometries were apparent from our simulations; one with the imidazole ring oriented parallel to the surface, and one with the ring arranged perpendicular to the surface plane, with the **de**-protonated nitrogen site weakly chemisorbing to the Au surface (see Figure S4). At the aqueous Au(111) interface, HisA adsorption features both orientations, while at the aqueous Au(100)(1×1) interface the perpendicular geometry dominates (see Figure S4).[37,38]

We **next** examined the effect of His **amino acid** protonation state on the binding strength. The difference in our predicted adsorption free energies of HisA and HisH at the Au(111) interface **was** modest at only 1.9 kJ mol^{-1}, in comparison with the 11.1 kJ mol^{-1} difference between the binding free energies for **tri-His** and **tri-Tyr**. For this reason, we suggest that the protonation state of **tri-His** is unlikely to affect the relative order of free energies of adsorption of the tri-peptides **on Au(111)** as predicted by simulation. **In contrast, our data suggest a clear difference in binding strength between HisA and HisH at the aqueous Au(100) interface, with HisA binding more strongly. Given the anticipated complexity of the protonation state ensemble (eight species) of tri-His in the adsorbed state, there is no clear-cut way to predict how these data practicably translate into a definitive binding strength ranking for tri-His in the Au(100)-adsorbed state when compared with the other two peptides which, at the amino acid level, are predicted to support reduced binding on Au(100) compared with Au(111). This statement should hold for any pH value but its**

interpretation may be particularly complex and nuanced for pH values in the range of 6-8.

The complexities of tri-His aside, we found that the choice of facet is predicted to strongly influence the binding strength of all four amino acids, with Tyr being the most profoundly affected. **On this basis, we suggest that** the relative differences in the adsorption free energies of the amino acids at the Au(111) and Au(100)(1×1) aqueous interfaces offer **one** plausible explanation for the weaker experimentally-determined YYY binding strength, relative to tri-His.[11] **To elaborate,** the Au NPs used by Cohavi *et al.* to decorate the SPR chip surface most likely presented a range of different Au facets, and in particular it is possible that, as low-energy crystallographic surface orientations, both the Au(111) and Au(100)(1×1) facets could have been available for peptide adsorption. Therefore, the weak adsorption of YYY to the native {100} facets may result in a weaker adsorption than **tri-His**, despite the fact that YYY adsorbs more strongly to the Au(111) interface. Based on these amino acid adsorption free energies and this two-facet approximation, **a naive estimate suggests that** a facet enrichment at a fraction greater than 57% Au(100)(1×1) of the total surface area in the SPR experiment, relative to a fraction of less than 43% Au(111), is predicted to yield a stronger adsorption free energy of **tri-His** relative to YYY. **However, this does not fully account for the true complexity of the tri-His protonation state ensemble. Certainly in the pH range of 6-8, the relative fraction of the eight possible tri-His species might vary sharply as a function of only minor changes to pH. Given our predictions of HisA and HisH amino acid binding strengths on the two Au facets, changes to these relative fractions may well have a strong impact on the resultant tri-His binding constant on the Au NP-decorated substrate.**

In addition to the different facets, the surface-immobilized Au NPs used in the SPR experiments would have also displayed low coordinate Au atoms at edge and vertex sites, which may also have weakened the overall binding strength of YYY relative to that of **tri-His**. *In vacuo* plane-wave density functional theory (PW-DFT) calculations have shown that

imidazole adsorbs more strongly to the edge and vertex sites of Au NPs than to the planar Au(111) surface.[76] In contrast, this same study found benzene (the closest analogue to Tyr; phenol was not investigated in this study) to adsorb more weakly to Au NPs at both the low-coordinate Au atom sites and both facets, compared with the infinite planar surfaces. While caution should be used when extrapolating from the results of *in vacuo* binding data to aqueous conditions, these previously-published DFT data support the hypothesis that the adsorption of YYY would be stronger at the aqueous Au(111) interface than at the surface of the Au NPs.

Both our simulations and the previously reported SPR experiments indicate tri-**Ser** to be the weakest-binding tri-peptide of the set. However, whereas the predicted Au-binding strength of SSS is significantly weaker than that of the other two tri-peptides, the experimentally-determined difference between the free-energies of adsorption of YYY and SSS was only 2.9 kJ mol^{-1}. The relatively stronger experimentally-determined binding of SSS is unlikely to be accounted for by the facet effects described above, because**, consistent with most experimental data to date,** our simulation data suggest that the free-energy of adsorption of Ser is weak at both the Au(111) and Au(100)(1×1) interfaces. However, the presence of NP vertices and edges may favor stronger Ser-Au interactions. *In vacuo* plane-wave density functional theory (PW-DFT) calculations indicate that the hydroxyl group adsorbs more strongly to the edge and vertex sites of Au NPs than to Au {111} or {100}.[76] In addition, as mentioned earlier, the **similarity in** the experimental binding strengths for YYY and SSS is surprising considering the consensus drawn from the current literature, from both experimental and simulation perspectives, in the sense that Tyr and His are thought to be strong binders of Au while Ser is not. This discrepancy **illustrates** the point that the current consensus on the Au-binding propensities of amino acids is evolving and will require further consolidation in future.

Some discussion of the calculations reported by Cohavi et al.[11] is warranted. These previous calculations considered the entire 3X-BLIP fusion protein and

its adsorption onto the Au(111) surface, and made use of the ProMetCS model.[77] These authors reported agreement between their experimentally-determined 'binding potency' (which, as explained earlier, is not necessarily a measure of binding constant) and a calculated relative-binding metric. The ProMetCS model is an approximate physics-based model that can be used to explore the surface-binding mechanisms of proteins. While ProMetCS is a fine model for such purposes, we believe the calculations of Cohavi et al.[11] did not make appropriate consideration of the limitations of the model. In the work of Cohavi et al.[11] these limitations in their calculations operated over two levels. First these authors assumed the 3X-BLIP binding energy could be partitioned into a BLIP-only and a 3X-only contribution, and furthermore, that the 3X-only term could be de-coupled into a sum of individual residue contributions, via use of a parameter (f) that was fitted to the experimental data. The current body of work in the field of peptide-surface adsorption refutes these assumptions. Second, the ProMetCS model has numerous limitations, including the use of the rigid body approximation (which cannot capture the surface-induced conformational change of the peptide), the lack of explicit solvent, and most critically, the known under- estimation of the metal desolvation energy for aromatic adsorbates.[77] This latter limitation could have an influential impact on the balance of the HisA/HisH/Tyr adsorption strengths. Moreover, Cohavi et al.[11] reported that their calculations could not reach agreement without modification of the surface charge density, which they stated was essentially a fitting parameter and not directly related to the surface charge under the experimental conditions. For these reasons, we do not seek to make a detailed comparison with the calculations reported by Cohavi et al.[11], given that in contrast to these ProMetCS calculations, our MD simulations explicitly capture the conformational, electrostatic and desolvation contributions of the binding free energy.

Facet-Specific Conformational Ensembles of Surface-Adsorbed Tri-Peptides

As explained in the Methodology, to determine the relative populations of the different conformations of the adsorbed tri-peptides **at the Au(111) and Au(100) aqueous interfaces**, a clustering analysis was performed for the reference replica trajectory of each tri-peptide. Each cluster identified in the analysis corresponds to a distinct group of structurally-similar backbone conformations of the adsorbed tri-peptide. In Figure S5 we provide the number of distinct clusters identified during the course of the REST MD simulations. These data show that by $\sim 9 \times 10^6$ REST MD steps, the number of clusters has plateaued, indicating that the simulations have approached equilibrium. The relative populations of the top-ten most populated clusters for each tri-peptide at the two interfaces are given in Table S1. Representative snapshots of the most populated clusters of each tri-peptide are shown in Figure 3 and Figure S6 for the Au(111) and Au(100)(1×1) interfaces. In all six simulations, the most populated cluster accounts for over 50% of the total population, with another two to four clusters possessing significant populations ($\geq 5\%$) also present.

We then investigated the degree of structural similarity in adsorbed conformations across the two facets. To do this, for all three tri-peptides, the structures of each of the five most populated clusters obtained for the Au(111) interface were compared against their counterparts adsorbed at the Au(100)(1×1) interface, by calculating the RMSD between the positions of backbone atoms between the cluster conformations. If the RMSD between a pair of structures was less than 0.5 Å (the cut-off distance used for the clustering analysis) then the two conformations were defined to be a structural match. The matches between structures adsorbed at the Au(111) and Au(100)(1×1) interfaces for the three tri-peptides are given in Table S2. Tri-serine showed the highest number of matches, with the top three clusters at both interfaces being matched, indicating that the conformational ensemble of this tri-peptide shared a high degree of similarity across the two interfaces.

The top two most populated conformations of **tri-His** were also matched across the

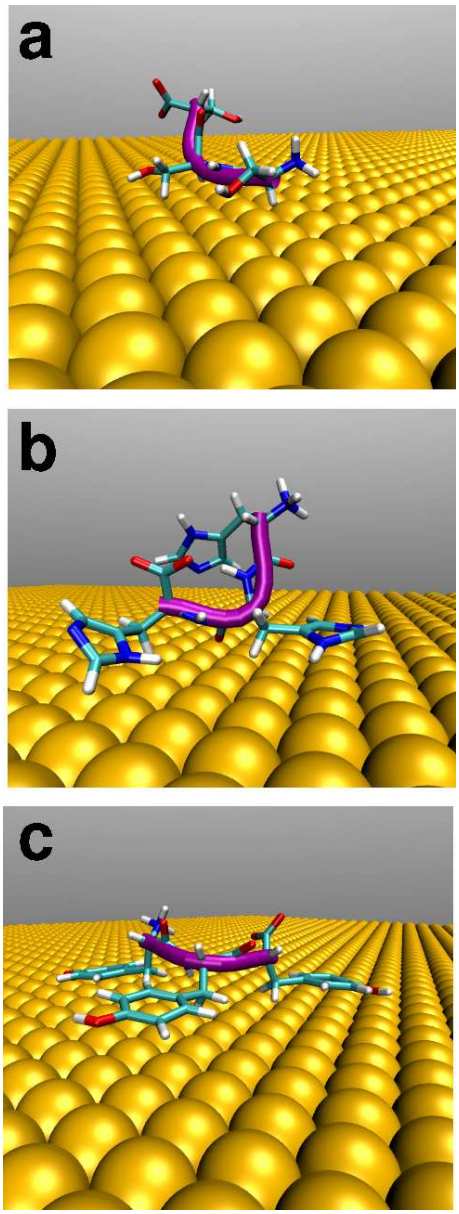

Figure 3: Representative snapshots of the most likely adsorbed conformations of the tri-peptides (a) tri-Ser, (b) tri-His and (c) tri-Tyr at the aqueous Au(111) interface. Water not shown for clarity.

Au(111) and Au(100)(1×1) interfaces, again indicating the similar *backbone* structure of this tri-peptide adsorbed at the two interfaces. In contrast, the most populated cluster of YYY adsorbed at the Au(111) interface **was** a match for the second-most populated cluster adsorbed at the Au(100)(1×1) interface, and *vice versa*. Considering that the most populated cluster of YYY accounts for 63/52 % of the total population at the Au(111)/(100)(1×1) interface, it is clear that the conformational ensemble of the YYY backbone is strongly affected by the structure of the Au interface.

Comparing the RMSD of the peptide backbone conformations of the initial structures with the representative structures of the top-five most populated clusters, we found a number of matches for all three peptides at both interfaces. For tri-His and tri-Ser, all of the initial structures were a match to at least one cluster at both interfaces, while for YYY at both interfaces there were just two initial structures that did not match at least one structure from the top-five most populated clusters. This degree of structural similarity is not surprising considering that the cumulative population of the top five clusters typically accounted for 95% of total ensemble. However, the relative population of any given cluster was not necessarily correlated with the number of matches found against the initial structures. For example, for YYY at Au(111) four of the initial conformations were a match to cluster 1, while nine of the initial conformations were a match to cluster 2. Therefore, the ensemble of initial conformations did not appear to bias the final conformational ensemble as determined from the REST simulations.

The degree of direct residue-surface contact calculated each residue of the tri-peptides is given in Figure 4, with the numerical data provided in Table S3 of the Supporting Information. Table S3 also indicates the degree of solvent-mediated contact for the Au(100)(1×1) surface. For all three tri-peptides, the **degree** of direct contact was diminished at the Au(100)(1×1) interface relative to that of Au(111), consistent with presence of the **more structured** first interfacial solvent layer. The two **de**-protonated His residues of **tri-His**

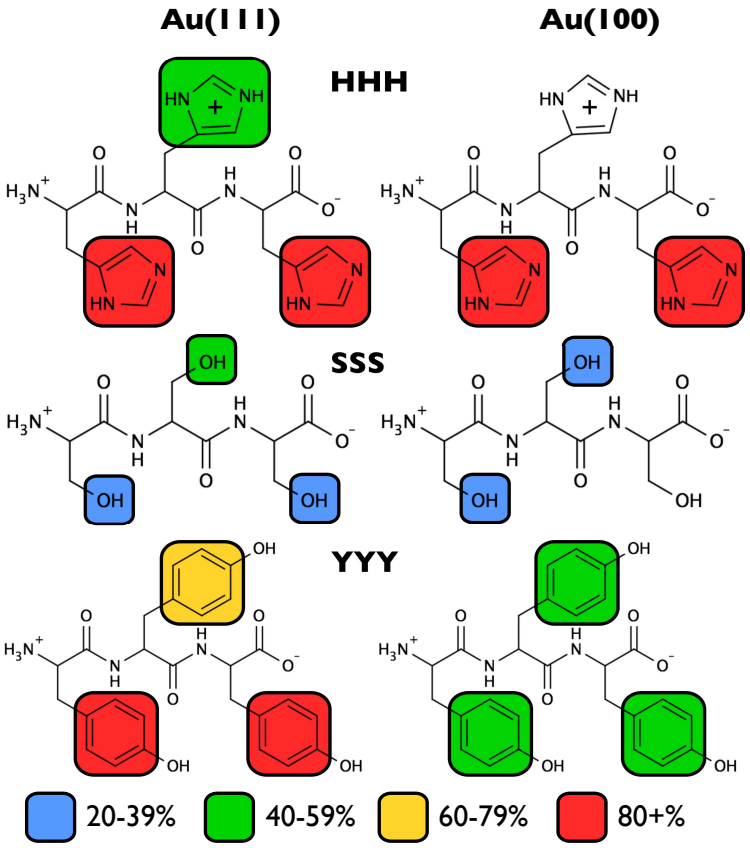

Figure 4: Degree of residue-surface contact for each of the tri-peptides adsorbed at the aqueous Au(111) and Au(100)(1×1) interfaces, predicted from REST simulations. Data for Au(100) are the combined direct- and solvent-mediated contact.

showed a high level of contact at both interfaces, while the central, protonated, His residue featured very little direct contact with the interface at the Au(100)(1×1) interface (consistent with the metadynamics simulations of the individual amino acids). At the Au(111) interface, H2, featured a moderate degree of contact, but was still less likely to be adsorbed than H1 or H3. This difference could be due to either the protonation state of the residues and/or the peptide structure. The simultaneous adsorption of all three His residues **was rare** and may sterically strain the peptide backbone. **Similarly,** YYY also showed a relatively reduced degree of contact for the central residue (*vide infra*), although in this instance all three residues could be found in a simultaneously-adsorbed state for 46 % of the trajectory. The full set of conditional probabilities for simultaneous multi-residue surface contact are provided in Table S4 of the Supporting Information.

Despite the similar degree of residue-surface contact calculated for H1 and H3, the mode of adsorption across the two interfaces **was** predicted to be quite different, apparent from the preferred tilt angle of the imidazole ring plane. At Au(111), the imidazole rings of H1 and H3 **were** more likely to lie flat (see Figure 3(b) and Figure S7(a) in the Supporting Information) while at Au(100)(1×1) the tilt angle of the rings is $\sim 90°$, indicating a perpendicular orientation mediated *via* the **de**-protonated nitrogen site (Figures S6(b) and S7(c) in the Supporting Information). While the conformations of the **tri-His** peptide backbone **share similarities across** the two facets, the orientation and position of the peptide backbone *with respect to the surface* is different in each case. At Au(111) the backbone lies relatively close to the surface, while in contrast, at Au(100)(1×1) the peptide backbone is more distant from the surface (Figure S8 in the Supporting Information).

As suggested by the predicted weaker adsorption, the degree of residue-surface contact calculated for **tri-Ser** at Au(111) is attenuated compared with that of **tri-His**, with **each of the** three Ser residues in direct contact with the Au interface for less than 50 % of the simulation trajectory. Simultaneous adsorption of **more than one** Ser residue was uncommon on both surfaces. Direct contact of the Ser residues with Au(100)(1×1) was minimal, with

solvent-mediated contact featuring at least as significantly as the direct contact mode (Figure S8(h)). A summation of the direct and solvent-mediated contact at the Au(100)(1×1) interface indicated significant, although weak, collective contact between the peptide and Au surfaces in general.

At the Au(111) aqueous interface, all three residues of YYY showed a strong degree of surface contact, although as seen for **tri-His**, the central residue was less likely to be found in direct contact compared with the terminal residues. Nevertheless, the simultaneous adsorption of all three residues on Au(111) was predicted for 46 % of the trajectory (Table S4), which indicates that the balance between the enthalpy gain for adsorption of the three rings and the possible energetic penalty incurred in straining the backbone to accommodate this favored the ring-surface interaction. When adsorbed at the Au(100)(1×1) aqueous interface, all three residues of YYY featured only moderate contact with the surface. As with the Au(111) surface, when adsorbed, all three Tyr side-chain rings were oriented parallel to the both the Au(111) and Au(100)(1×1) planes (Figure S7 in the Supporting Information). At the Au(100)(1×1) interface, the relatively weaker residue-surface interaction meant that adsorption of the tri-peptide in a conformation equivalent to the most populated cluster at the Au(111) interface was unfavorable. When adsorbed, all three phenol rings lay parallel to the both the Au(111) and Au(100)(1×1) interfaces (Figure S7, Supporting Information).

Our findings **indicate** the **relevance** of considering different facets, and their different surface reconstructions, in simulation studies where appropriate, for comparison with experimental studies where the target substrate comprises Au NPs. Our results also indicate how facet-selective adsorption could be exploited for nanomaterials generation, such as using additives to mediate shape-selective Au NP synthesis in aqueous media.[78,79] Previous experimental work has shown that water-based peptide-mediated Au NP synthesis without a seed nanoparticle is not shape selective.[80] However, studies of Pt NP synthesis in aqueous media indicated that peptides could direct the production of shape-controlled NPs using seeded growth,[81,82] which suggests that a similar strategy could be successful for Au NPs.

Moreover, a peptide-mediated strategy for shaped NP growth could also be used to direct the one-pot production and organization of NPs into assemblies.[44]

Our simulations also highlight the structural consequences of protonation state of the His residues, particularly at the Au(100)(1×1) facet. The protonation state of His when adsorbed at an aqueous Au interface may differ from that in solution, and may also be facet-specific. Experimental investigation of the protonation state of His residues at different Au interfaces would be highly valuable in **bridging** the gap between experiment and simulation.

Conclusions

Via a combination of simulation approaches, together with a consideration of different surface structural models, our findings can **explore and contrast** recent surface plasmon resonance **(SPR)** spectroscopy **measurements** of homo-tri-peptide binding **constants** at the aqueous Au interface. Using metadynamics simulations, we predicted the adsorption free energies of three homo-tri-peptides **at aqueous** Au(111) and ranked these, finding YYY > HHH > SSS. However, this predicted ranking differed with the SPR-determined ranking reported **for these tri-peptides adsorbed at a target Au substrate comprising surface-immobilized Au NPs,** which suggested HHH > YYY > SSS. We propose that **one possible source of** discrepancy in **the** relative ordering of **the** HHH and YYY **tri-peptide** binding constants between simulation and experiment **may arise** from the presence of facets other than the Au(111) surface, that are typically present on Au nanoparticles. Metadynamics simulations of the HisA, HisH, Tyr and Ser amino acids adsorbed at the aqueous Au(111) and Au(100)(1×1) interfaces support this hypothesis, predicting the binding strength of the Tyr **amino acid** to be substantial at the Au(111) interface but negligible at the Au(100)(1×1) interface. **HisH showed a similar trend to Tyr, while in contrast, HisA featured a relatively smaller** corresponding drop in binding strength between the Au(111) and Au(100) interfaces. **However, we suggest that complexities arising from**

the ensemble of possible protonation states for the tri-His peptide present an additional challenge for the unambiguous prediction and interpretation of binding constants at the aqueous Au interface, particularly at neutral pH. Also, our REST-MD simulations revealed facet-specific differences in the binding modes of these three tri-peptides. In general, the Au(111) interface promoted direct residue-surface contact, while solvent-mediated contact was favored on Au(100)(1×1). Overall, **our** findings advance our understanding of how the adsorption of peptides **might** be modulated by the presence of different Au facets. This deeper **comprehension** of peptide-materials structure/property relationships is needed to fully realize the true potential of functional materials based on biotic/abiotic interfaces.

Acknowledgement

The authors thank the Victorian Life Sciences Computation Initiative (VLSCI) for computational resources. This work was supported in part by by the Air Office of Scientific Research, grant number FA9550-12-1-0226.

Supporting Information Available

Free-energies of adsorption of tri-peptides over time; collective variable of tri-peptide metadynamics simulations over time; snapshots of His and Ser amino acids at the Au(111) and Au(100)(1×1) interfaces; exemplar REST replica mobilities; number of cluster of tri-peptides identified from REST simulations; representative snapshots of the tri-peptides at the Au(100)(1×1) interface; cluster populations from REST simulations; residue-surface contact percentages from REST simulations; ring tilt angles of HHH and YYY from REST simulations. This material is available free of charge via the Internet at `http://pubs.acs.org/`.

References

(1) Care, A.; Bergquist, P. L.; Sunna, A. Solid-binding Peptides: Smart Tools for Nanobiotechnology. *Trends Biotechnol.* **2015**, *33*, 259–268.

(2) Hnilova, M.; Karaca, B. T.; Park, J.; Jia, C.; Brandon, W. R.; Sarikaya, M.; Tamerler, C. Fabrication of Hierarchical Hybrid Structures UsingBio-Enabled Layer-by-Layer Self-Assembly. *Biotech. Bioeng.* **2012**, *109*, 1120–1130.

(3) Hnilova, M.; So, C. R.; Oren, E. E.; Wilson, B. R.; Kacar, T.; Tamerler, C.; Sarikaya, M. Peptide-directed Co-assembly of Nanoprobes on Multimaterial Patterned Solid Surfaces. *Soft Matter* **2012**, *8*, 4327–4334.

(4) Bedford, N. M.; Hughes, Z. E.; Tang, Z.; Li, Y.; Briggs, B. D.; Ren, Y.; Swihart, M. T.; Petkov, V. G.; Naik, R. R.; Knecht, M. R.; Walsh, T. R. Sequence-Dependent Structure/Function Relationships of Catalytic Peptide-Enabled Gold Nanoparticles Generated under Ambient Synthetic Conditions. *J. Am. Chem. Soc.* **2016**, *138*, 540–548.

(5) Zhou, W.; Gao, X.; Liu, D.; Chen, X. Gold Nanoparticles for In Vitro Diagnostics. *Chem. Rev.* **2015**, *115*, 10575–10636.

(6) Chakraborty, M.; Jain, S.; Rani, V. Nanotechnology:Emerging Tool for Diagnostics and Therapeutics. *Appl. Biochem. Biotechnol.* **2011**, *165*, 1178–1187.

(7) Mahmood, M.; Casciano, D.; Xu, Y.; Birisi, A. S. Engineered Nanostructural Materials for Application in Cancer Biology and Medicine. *J. Appl. Toxicol.* **2011**, *32*, 10–19.

(8) Kumar, A.; Ma, H.; Zhang, X.; Huang, K.; Jin, S.; Liu, J.; Wei, T.; Cao, W.; Zou, G.; Liang, X.-J. Gold Nanoparticles Functionalized with Therapeutic and Targeted Peptides for Cancer Treatment. *Biomaterials* **2012**, *33*, 1180–1189.

(9) Webb, J. A.; Bardhan, R. Emerging Advances in Nanomedicine with Engineered Gold Nanostructures. *Nanoscale* **2014**, *6*, 2502–2530.

(10) Hnilova, M.; Oren, E. E.; Seker, U. O. S.; Wilson, B. R.; Collino, S.; Evans, J. S.; Tamerler, C.; Sarikaya, M. Effect of Molecular Conformations on the Adsorption Behavior of Gold-Binding Peptides. *Langmuir* **2008**, *24*, 12440–12445.

(11) Cohavi, O.; Reichmann, D.; Abramovich, R.; Tesler, A. B.; Bellapadrona, G.; Kokh, D. B.; Wade, R. C.; Vaskevich, A.; Rubinstein, I.; Schreiber, G. A Quantitative, Real-Time Assessment of Binding of Peptides and Proteins to Gold Surfaces. *Chem. Eur. J.* **2010**, *17*, 1327–1336.

(12) Tang, Z.; Palafox-Hernandez, J. P.; Law, W.-C.; Hughes, Z. E.; Swihart, M. T.; Prasad, P. N.; Knecht, M. R.; Walsh, T. R. Biomolecular Recognition Principles for Bionanocombinatorics: An Integrated Approach To Elucidate Enthalpic and Entropic Factors. *ACS Nano* **2013**, *7*, 9632–9646.

(13) Palafox-Hernandez, J. P.; Lim, C.-K.; Tang, Z.; Drew, K. L. M.; Hughes, Z. E.; Li, Y.; Swihart, M. T.; Prasad, P. N.; Knecht, M. R.; Walsh, T. R. Optical Actuation of Inorganic/Organic Interfaces: Comparing Peptide-Azobenzene Ligand Reconfiguration on Gold and Silver Nanoparticles. *ACS Appl. Mater. Interfaces* **2016**, *8*, 1050–1060.

(14) Munro, C. E.; Hughes, Z. E.; Walsh, T. R.; Knecht, M. R. Peptide Sequence Effects Control the Single Pot Reduction, Nucleation, and Growth of Au Nanoparticles. *J. Phys. Chem. C* **2016**, *120*, 18917–18924.

(15) Li, H.-Q.; Chen, A.; G Roscoe, S.; Lipkowski, J. Electrochemical and FTIR Studies of L-phenylalanine Adsorption at the Au (111) Electrode. *J. Electroanal. Chem.* **2001**, *500*, 299–310.

(16) Ju, S.; Yeo, W. S. Quantification of Proteins on Gold Nanoparticles by Combining MALDI-TOF MS and Proteolysisxs. *Nanotechnology* **2012**, *23*, 135701–135708.

(17) Sultan, A. M.; Westcott, Z. C.; Hughes, Z. E.; Palafox-Hernandez, J. P.; Giesa, T.; Puddu, V.; Buehler, M. J.; Perry, C. C.; Walsh, T. R. Aqueous Peptide-TiO_2 Interfaces:

Iso-energetic Binding via either Entropically- or Enthalpically-driven Mechanisms. *ACS Appl. Mater. Interfaces* **2016**, *8*, 18620–18630.

(18) So, C. R.; Tamerler, C.; Sarikaya, M. Adsorption, Diffusion, and Self-Assembly of an Engineered Gold-Binding Peptide on Au(111) Investigated by Atomic Force Microscopy. *Angew. Chem. Int. Ed.* **2009**, *48*, 5174–5177.

(19) Deng, Z.; Thontasen, N.; Malinowski, N.; Rinke, G.; Harnau, L.; Rauschenbach, S.; Kern, K. A Close Look at Proteins: Submolecular Resolution of Two- and Three-Dimensionally Folded Cytochrome C at Surfaces. *Nano Lett.* **2012**, *12*, 2452–2458.

(20) Chen, C.-L.; Zuckermann, R. N.; DeYoreo, J. J. Surface-Directed Assembly of Sequence-Defined Synthetic Polymers into Networks of Hexagonally Patterned Nanoribbons with Controlled Functionalities. *ACS Nano* **2016**, *10*, 5314–5320.

(21) Calzolai, L.; Franchini, F.; Gilliland, D.; Rossi, F. Protein-Nanoparticle Interaction:Identification of the Ubiquitin-Gold Nanoparticle Interaction Site. *Nano Lett.* **2010**, *10*, 3101–3105.

(22) Mirau, P. A.; Naik, R. R.; Gehring, P. Structure of Peptides on Metal Oxide Surfaces Probed by NMR. *J. Am. Chem. Soc.* **2011**, *133*, 18243–18248.

(23) Ye, S.; Li, H.; Yang, W.; Luo, Y. Accurate Determination of Interfacial Protein Secondary Structure by Combining Interfacial-Sensitive Amide I and Amide III Spectral Signals. *J. Am. Chem. Soc.* **2014**, *136*, 1206–1209.

(24) So, C. R.; Liu, J.; Fears, K. P.; Leary, D. H.; Golden, J. P.; Wahl, K. J. Self-Assembly of Protein Nanofibrils Orchestrates Calcite Step Movement through Selective Nonchiral Interactions. *ACS Nano* **2015**, *9*, 5782–5791.

(25) Baker, C. M.; Best, R. B. Insights Into the Binding of Intrinsically Disordered Proteins from Molecular Dynamics Simulation. *WIREs Comput. Mol. Sci.* **2013**, *4*, 182–198.

(26) van der Lee, R. et al. Classification of Intrinsically Disordered Regions and Proteins. *Chem. Rev.* **2014**, *114*, 6589–6631.

(27) Braun, R.; Sarikaya, M.; Schulten, K. Genetically Engineered Au-binding Polypeptides: Structure Prediction and MD. *J. Biomater. Sci. Polymer Edn.* **2002**, *13*, 747.

(28) Ghiringhelli, L. M.; Hess, B.; van der Vegt, N. F. A.; Site, L. D. Competing Adsorption between Hydrated Peptides and Water onto Metal Surfaces: From Electronic to Conformational Properties. *J. Amer. Chem. Soc.* **2008**, *130*, 13460–13464.

(29) Heinz, H.; Farmer, B. L.; Pandey, R. B.; Slocik, J. M.; Patnaik, S. S.; Pachter, R.; Naik, R. R. Nature of Molecular Interactions of Peptides with Gold, Palladium, and Pd-Au Bimetal Surfaces in Aqueous Solution. *J. Am. Chem. Soc.* **2009**, *131*, 9704–9714.

(30) Hoefling, M.; Iori, F.; Corni, S.; Gottschalk, K.-E. Interaction of Amino Acids with the Au(111) Surface: Adsorption Free Energies from Molecular Dynamics Simulations. *Langmuir* **2010**, *26*, 8347–8351.

(31) Yu, J.; Becker, L.; Carri, G. A. A Molecular Dynamics Simulation of the Stability Limited Growth Mechanism of Peptide- Mediated Gold-Nanoparticle Synthesis. *Small* **2010**, *6*, 2242–2245.

(32) Feng, J.; Pandey, R. B.; Berry, R. J.; Farmer, B. L.; Naik, R. R.; Heinz, H. Adsorption Mechanism of Single Amino Acid and Surfactant Molecules to Au(111) Surafces in Aquoues Solution:Design rules for Metal-Binding Molecules. *Soft Matter* **2011**, *7*, 2113–2120.

(33) Heinz, H.; Jha, K. C.; Luettmer-Strathmann, J.; Farmer, B. L.; ; Naik, R. R. Polarization at Metal-Biomolecular Interfaces in Solution. *J. R. Soc. Interface* **2011**, *8*, 220–232.

(34) Vila Verde, A.; Beltramo, P. J.; Maranas, J. K. Adsorption of Homopolypeptides on Gold Investigated Using Atomistic Molecular Dynamics. *Langmuir* **2011**, *27*, 5918–5926.

(35) Yu, J.; Becker, L.; Carri, G. A. The Influence of Amino Acid Sequence and Functionality on the Binding Process of Peptides onto Gold Surfaces. *Langmuir* **2012**, *28*, 1408–1417.

(36) Corni, S.; Hnilova, M.; Tamerler, C.; Sarikaya, M. Conformational Behavior of Genetically-Engineered Dodecapeptides as a Determinant of Binding Affinity for Gold. *J. Phys. Chem. C* **2013**, *117*, 16990–17003.

(37) Wright, L. B.; Rodger, P. M.; Walsh, T. R.; Corni, S. First-Principles-Based Force Field for the Interaction of Proteins with Au(100)(5×1): An Extension of GolP-CHARMM. *J. Phys. Chem. C* **2013**, *117*, 24292–24306.

(38) Wright, L. B.; Rodger, P. M.; Corni, S.; Walsh, T. R. GolP-CHARMM: First-Principles Based Force-fields for the Interaction of Proteins with Au(111) and Au(100). *J. Chem. Theory Comput.* **2013**, *9*, 1616–1630.

(39) Palafox-Hernandez, J. P.; Tang, Z.; Hughes, Z. E.; Li, Y.; Swihart, M. T.; Prasad, P. N.; Walsh, T. R.; Knecht, M. R. Comparative Study of Materials-Binding Peptide Interactions with Gold and Silver Surfaces and Nanostructures: A Thermodynamic Basis for Biological Selectivity of Inorganic Materials. *Chem. Mater.* **2014**, *26*, 4960–4969.

(40) Nawrocki, G.; Cieplak, M. Aqueous Amino Acids and Proteins Near the Surface of Gold in Hydrophilic and Hydrophobic Force Fields. *J. Phys. Chem. C* **2014**, *118*, 12929–12943.

(41) Wright, L. B.; Palafox-Hernandez, J. P.; Rodger, P. M.; Corni, S.; Walsh, T. R. Facet Selectivity in Gold Binding Peptides: Exploiting Interfacial Water Structure. *Chem. Sci.* **2015**, *6*, 5204–5214.

(42) Charchar, P.; Christofferson, A. J.; Todorova, N.; Yarovsky, I. Understanding and Designing the Gold-Bio Interface: Insights from Simulations. *Small* **2016**, *12*, 2395–2418 .

(43) Ozboyaci, M.; Kokh, D. B.; Wade, R. C. Three Steps to Gold: Mechanism of Protein Adsorption Revealed by Brownian and Molecular Dynamics Simulations. *Phys. Chem. Chem. Phys.* **2016**, *18*, 10191–10200.

(44) Briggs, B. D.; Palafox-Hernandez, J. P.; Li, Y.; Lim, C.-K.; Woehl, T. J.; Bedford, N. M.; Seifert, S.; Swihart, M. T.; Prasad, P. N.; Walsh, T. R.; Knecht, M. R. Toward a Modular Multi-material Nanoparticle Synthesis and Assembly Strategy via Bionanocombinatorics: Bifunctional Peptides for Linking Au and Ag Nanomaterials. *Phys. Chem. Chem. Phys.* **2016**, *18*, 30845–30856.

(45) Bedford, N. M.; Showalter, A. R.; Woehl, T. J.; Hughes, Z. E.; Lee, S.; Reinhart, B.; Ertem, S. P.; Coughlin, E. B.; Ren, Y.; Walsh, T. R.; Bunker, B. A. Peptide-Directed PdAu Nanoscale Surface Segregation: Toward Controlled Bimetallic Architecture for Catalytic Materials. *ACS Nano* **2016**, *10*, 8645–8659.

(46) Iori, F.; Di Felice, R.; Molinari, E.; Corni, S. GolP: An Atomistic Force-field to Describe the Interaction of Proteins with Au(111) Surfaces in water. *J. Comput. Chem.* **2009**, *30*, 1465–1476.

(47) Heinz, H.; Lin, T.-J.; Kishore Mishra, R.; Emami, F. S. Thermodynamically Consistent Force Fields for the Assembly of Inorganic, Organic, and Biological Nanostructures: The INTERFACE Force Field. *Langmuir* **2013**, *29*, 1754–1765.

(48) MacKerell, A. D., Jr; Bashford, D.; Bellott, M.; Dunbrack, R. L., Jr; Evanseck, J. D.; Field, M. J.; Fischer, S.; Gao, J.; Guo, H.; Ha, S. All-atom Empirical Potential for Molecular Modeling and Dynamics Studies of Proteins. *J. Phys. Chem. B* **1998**, *102*, 3586–3616.

(49) Piana, S.; Lindorff-Larsen, K.; Shaw, D. E. How Robust Are Protein Folding Simulations with Respect to Force Field Parameterization? *Biophys. J.* **2011**, *100*, L47–L49.

(50) Barducci, A.; Bussi, G.; Parrinello, M. Well-tempered Metadynamics: A Smoothly Converging and Tunable Free-energy Method. *Phys. Rev. Lett.* **2008**, *100*, 020603.

(51) Terakawa, T.; Kameda, T.; Takada, S. On Easy Implementation of a Variant of the Replica Exchange with Solute Tempering in GROMACS. *J. Comput. Chem.* **2010**, *32*, 1228–1234.

(52) Wright, L. B.; Walsh, T. R. Efficient Conformational Sampling of Peptides Adsorbed onto Inorganic Surfaces: Insights from a Quartz binding Peptide. *Phys. Chem. Chem. Phys.* **2013**, *15*, 4715–4726.

(53) Hughes, Z. E.; Walsh, T. R. Structure of the Electrical Double Layer at Aqueous Gold and Silver Interfaces for Saline Solutions. *J. Colloid Interface Sci.* **2014**, *436*, 99–110.

(54) Hughes, Z. E.; Nguyen, M.; Li, Y.; Swihart, M. T.; Walsh, T. R.; Knecht, M. R. Elucidating the Influence of Materials-Binding Peptide Sequence on Au Surface Interactions and Colloidal Stability of Au Nanoparticles. *Nanoscale* **2017**, *9*, 421–432.

(55) Willett, R. L.; Baldwin, K. W.; West, K. W.; Pfeiffer, L. N. Differential Adhesion of Amino Acids to Inorganic Surfaces. *Proc. Nat. Acad. Sci.* **2005**, *102*, 7817–7822.

(56) Peelle, B. R.; Krauland, E. M.; Wittrup, K. D.; Belcher, A. M. Design Criteria for Engineering Inorganic Material-specific Peptides. *Langmuir* **2005**, *21*, 6929–6933.

(57) Tan, Y. N.; Lee, J. Y.; Wang, D. I. C. Uncovering the Design Rules for Peptide Synthesis of Metal Nanoparticles. *J. Amer. Chem. Soc.* **2010**, *132*, 5677–5686.

(58) Vellore, N. A.; Yancey, J. A.; Collier, G.; Latour, R. A.; Stuart, S. J. Assessment of the Transferability of a Protein Force Field for the Simulation of Peptide-Surface Interactions. *Langmuir* **2010**, *26*, 7396–7404.

(59) Deighan, M.; Pfaendtner, J. Exhaustively Sampling Peptide Adsorption with Metadynamics. *Langmuir* **2013**, *29*, 7999–8009.

(60) Meißner, R. H.; Schneider, J.; Schiffels, P.; Colombi Ciacchi, L. Computational Prediction of Circular Dichroism Spectra and Quantification of Helicity Loss upon Peptide Adsorption on Silica. *Langmuir* **2014**, *30*, 3487–3494.

(61) Levine, Z. A.; Fischer, S. A.; Shea, J.-E.; Pfaendtner, J. Trp-Cage Folding on Organic Surfaces. *J. Phys. Chem. B* **2015**, *119*, 10417–10425.

(62) Nosé, S. A Unified Formulation of the Constant Temperature Molecular Dynamics Methods. *J. Chem. Phys.* **1984**, *81*, 511–519.

(63) Hoover, W. Canonical dynamics: Equilibrium phase-space distributions. *Phys. Rev. A* **1985**, *31*, 1695–1697.

(64) Jorgensen, W. L.; Chandrasekhar, J.; Madura, J. D.; Impey, R. W.; Klein, M. L. Comparison of Simple Potential Functions for Simulating Liquid Water. *J. Chem. Phys.* **1983**, *79*, 926–935.

(65) Neria, E.; Fischer, S.; Karplus, M. Simulation of Activation Free Energies in Molecular Systems. *J. Chem. Phys.* **1996**, *105*, 1902–1921.

(66) Wright, L. B.; Freeman, C. L.; Walsh, T. R. Benzene Adsorption at the Aqueous (011) Alpha-quartz Interface: Is Surface Flexibility Important? *Mol. Simulat.* **2013**, *39*, 1093–1102.

(67) Hess, B.; Kutzner, C.; Van Der Spoel, D.; Lindahl, E. GROMACS 4: Algorithms for Highly Efficient, Load-Balanced, and Scalable Molecular Simulation. *J. Chem. Theory Comput.* **2008**, *4*, 435–447.

(68) Darden, T.; York, D.; Pedersen, L. Particle Mesh Ewald - an N.Log(N) Method for Ewald Sums in Large Systems. *J. Chem. Phys.* **1993**, *98*, 10089–10092.

(69) Sprenger, K. G.; He, Y.; Pfaendtner, J. *Foundations of Molecular Modeling and Simulation*; Springer Singapore, 2016; Chapter Probing How Defects in Self-assembled Monolayers Affect Peptide Adsorption with Molecular Simulation, pp 21–35.

(70) Bonomi, M.; Branduardi, D.; Bussi, G.; Camilloni, C.; Provasi, D.; Raiteri, P.; Donadio, D.; Marinelli, F.; Pietrucci, F.; Broglia, R. A. PLUMED: A Portable Plugin for Free-energy Calculations with Molecular Dynamics. *Comput. Phys. Comm.* **2009**, *180*, 1961–1972.

(71) Schneider, J.; Colombi Ciacchi, L. Specific Material Recognition by Small Peptides Mediated by the Interfacial Solvent Structure. *J. Am. Chem. Soc.* **2012**, *134*, 2407.

(72) Daura, X.; Gademann, K.; Jaun, B.; Seebach, D.; van Gunsteren, W. F.; Mark, A. E. Peptide Folding: When Simulation Meets Experiment. *Angew. Chem. Int. Ed.* **1999**, *38*, 236–240.

(73) Desmond, J. L.; Rodger, P. M.; Walsh, T. R. Testing the inter-operability of the CHARMM and SPC/Fw force fields for conformational sampling. *Mol. Simulat.* **2014**, *40*, 912–921.

(74) Khandogin, J.; Brooks, C. L. Toward the Accurate First-principles Prediction of Ionization Equilibria in Proteins. *Biochemistry* **2006**, *45*, 9363–9373.

(75) Limmer, D. T.; Willard, A. P.; Madden, P.; Chandler, D. Hydration of Metal Surfaces can be Dynamically Heterogeneous and Hydrophobic. *Proc. Natl. Acad Sci.* **2013**, *110*, 4200–4205.

(76) Hughes, Z. E.; Walsh, T. R. Non-covalent Adsorption of Amino Acid Analogues on Noble-metal Nanoparticles: Influence of Edges and Vertices. *Phys. Chem. Chem. Phys.* **2016**, *18*, 17525–17533.

(77) Kokh, D. B.; Corni, S.; Winn, P. J.; Hoefling, M.; Gottschalk, K. E.; Wade, R. C. ProMetCS: An Atomistic Force Field for Modeling Protein-Metal Surface Interactions in a Continuum Aqueous Solvent. *J. Chem. Theory Comput.* **2010**, *6*, 1753–1768.

(78) Meena, S. K.; Celiksoy, S.; Schaefer, P.; Henkel, A.; Soennichsen, C.; Sulpizi, M. The Role of Halide Ions in the Anisotropic Growth of Gold Nanoparticles: A Microscopic, Atomistic Perspective. *Phys. Chem. Chem. Phys.* **2016**, *18*, 13246–13254.

(79) Meena, S. K.; Sulpizi, M. From Gold Nanoseeds to Nanorods: The Microscopic Origin of the Anisotropic Growth. *Angew. Chem. Int. Ed.* **2016**, *55*, 11960 –11964.

(80) Li, Y.; Tang, Z.; Prasad, P. N.; Knecht, M. R.; Swihart, M. T. Peptide-mediated Synthesis of Gold Nanoparticles: Effects of Peptide Sequence and Nature of Binding on Physicochemical Properties. *Nanoscale* **2014**, *6*, 3165–3172.

(81) Forbes, L. M.; Goodwin, A. P.; Cha, J. N. Tunable Size and Shape Control of Platinum Nanocrystals from a Single Peptide Sequence. *Chem. Mater.* **2010**, *22*, 6524–6528.

(82) Chiu, C.-Y.; Li, Y.; Ruan, L.; Ye, X.; Murray, C. B.; Huang, Y. Platinum Nanocrystals Selectivity Shaped Using Facet-specific Peptide Sequences. *Nature Chem.* **2011**, *3*, 393–399.

Graphical TOC Entry